LA-12720-MS

UC-814
Issued: April 1994

Calcite Deposits in Drill Cores USW G-2 and USW GU-3/G-3 at Yucca Mountain, Nevada:

Preliminary Report

David T. Vaniman

Los Alamos
NATIONAL LABORATORY
Los Alamos, New Mexico 87545

CALCITE DEPOSITS IN DRILL CORES USW G-2 AND USW GU-3/G-3 AT YUCCA MOUNTAIN, NEVADA: PRELIMINARY REPORT

by

D. T. Vaniman

ABSTRACT

Chemical and petrographic studies of fracture calcites in drill cores USW G-2 and USW GU-3/G-3 from Yucca Mountain, Nevada, provide evidence that (1) shallow fracture calcites generally have prominent negative Ce and Eu anomalies and low transition-metal contents that distinguish them from deeper calcites and that (2) there is significant variability among shallow fracture calcites, even though they are more closely related to each other than to the deeper calcites. The boundary between shallow and deep calcites corresponds roughly to the present static water level (SWL). The deep calcites appear to be derived from fluids enriched in some transition metals and are unaffected by dissolution/precipitation reactions that can lead to enlarged negative Eu and Ce anomalies. In contrast, most if not all of the shallow calcites are modified by such processes and may be derived from surface waters. The causes of variability among shallow calcites of these two drill cores are less evident, but may reflect competition with other minerals for certain trace elements during calcite precipitation, incongruent dissolution of source rocks in the formation of the calcite-precipitating fluids, and perhaps other processes not apparent in the data that have been collected so far.

Introduction

Yucca Mountain is being studied as a potential site for deep geologic disposal of high-level radioactive waste. Should a repository be developed at Yucca Mountain, the preferred location is within the upper unsaturated tuffaceous volcanic rocks. In this location, one factor of concern is the amount and rate of aqueous transport through the unsaturated rocks toward the underlying saturated intervals. Calcite, one of the most recently-formed minerals at Yucca Mountain, is of minor abundance in the unsaturated rocks but is widely distributed. Studies of calcite ages, isotopic systematics, chemistry and petrography could lead to a better understanding of transport processes at Yucca Mountain. Specifically, the study of past calcite precipitation can provide a variety of key data:

- Calcite deposits are markers of where water has been in the unsaturated rocks; preferred pathways may be marked by calcite deposits.
- Dated calcite deposits indicate when water was there.
- In some cases, models of carbonate transport and precipitation may allow estimation of minimum quantities of flow.
- Reconstructions of the aqueous chemical environments of most recent calcite deposition may be used to predict potential future coprecipitation of waste with carbonate and associated minerals (*e.g.*, opal and sepiolite) at Yucca Mountain.

Calcite occurs in a variety of forms and fabrics at Yucca Mountain. A shallow horizontal core at Fran Ridge, just east of Yucca Mountain, revealed that calcite within approximately 9 m of the surface is microcrystalline and similar to pedogenic forms (Norris *et al.*, 1986). Current studies of calcite in cores indicate that calcified or silicified root fossils commonly associated with pedogenic

features can be found to depths at least as great as 16 m. Deeper calcites are coarse and euhedral where fracture faces and cavity interiors are open; in the devitrified welded tuffs, the surfaces of both open fractures and lithophysal cavities may be coated by euhedral calcite crystals. Some penetration of calcite into the tuff matrix may also occur. Matrix calcite is most prominent, however, in some of the porous vitric-nonwelded intervals above the static water level (SWL), particularly in the nonwelded zone immediately above the Topopah Spring Member of the Paintbrush Tuff. Calcite is relatively rare in the interval that extends from the SWL to 200-300 m beneath the SWL; at greater depths, however, calcite is commonly found as fillings within sealed fractures, as a matrix mineral, and in zones of albite alteration as a replacement of pumice, shards, and feldspar phenocrysts. As a fracture mineral, calcite is more abundant in fractures crossing devitrified tuffs than in those that cross zeolitized tuffs (Carlos, 1987).

Preliminary data on the ages of fracture- and cavity-filling calcites at Yucca Mountain have been summarized by Szabo and Kyser (1990). Using uranium-series dating, they inferred episodic deposition of most calcite above the SWL during meteoric recharge episodes occurring within the past 400 Ka. They further suggested that distinct calcite precipitation episodes may have been concentrated at 28, 170, and 280 Ka. The apparent absence of U exchange between calcite and associated opal supports their conclusion that these calcite ages have not been modified by open-system processes.

Whelan and Stuckless (1992) found that the $\delta^{13}C$ compositions of calcites differ markedly above and below the SWL, with lighter carbon ($\delta^{13}C$ of -9.5 to -4‰) in the unsaturated zone and heavier carbon ($\delta^{13}C$ of -2 to 3‰) in the saturated zone. The carbon isotope data indicate that the calcites above the SWL precipitated from waters that had reacted with the overlying soils and plants, whereas the calcites beneath the SWL precipitated from waters of the deeper Paleozoic aquifer, although there is considerable overlap of the two $\delta^{13}C$ groups in a zone from 300 m below to 500 m above the present SWL. Strontium isotope data on the calcites (Peterman *et al.*, 1992) reinforce the fundamental distinctions between calcites above and below the SWL. Calcites of the unsaturated zone within 400 m of the surface have more radiogenic Sr ($^{87}Sr/^{86}Sr$ av. 0.71215) than those below the SWL ($^{87}Sr/^{86}Sr$ av. 0.70909). Intermediate $^{87}Sr/^{86}Sr$ values occur in the unsaturated zone within 100 m of the SWL, perhaps related to past rise in the water table.

In this paper the chemistry and petrography of calcites from fractures both above and below the present SWL are described. The data presented are for the northernmost deep drill core at Yucca Mountain, USW G-2, and the southernmost, USW GU-3/G-3. Figure 1 shows the locations of the fracture calcites studied from these two drill cores relative to the distribution and abundance of calcite within bulk-rock samples. A few preliminary data have also been collected from cores USW G-1 and USW G-4 (Vaniman, 1993), and work is in progress on other core samples. These data are considered in this report but are not discussed in detail. Further reports will provide more detailed analysis as more data become available.

Calcite distributions in USW G-2 and USW GU-3/G-3

Bulk-rock samples from drill core USW G-2 contain atypically large amounts of calcite in some parts of the unsaturated zone, with abundances as great as 20% in portions of devitrified tuff near the surface and as great as 40% in nonwelded vitric tuff at 207-230 m depth (Bish and Chipera, 1989). Calcite becomes essentially ubiquitous at depth in USW G-2, from about 666 m below the present SWL to the bottom of the drill core (1831 m depth). Throughout this deeper zone the

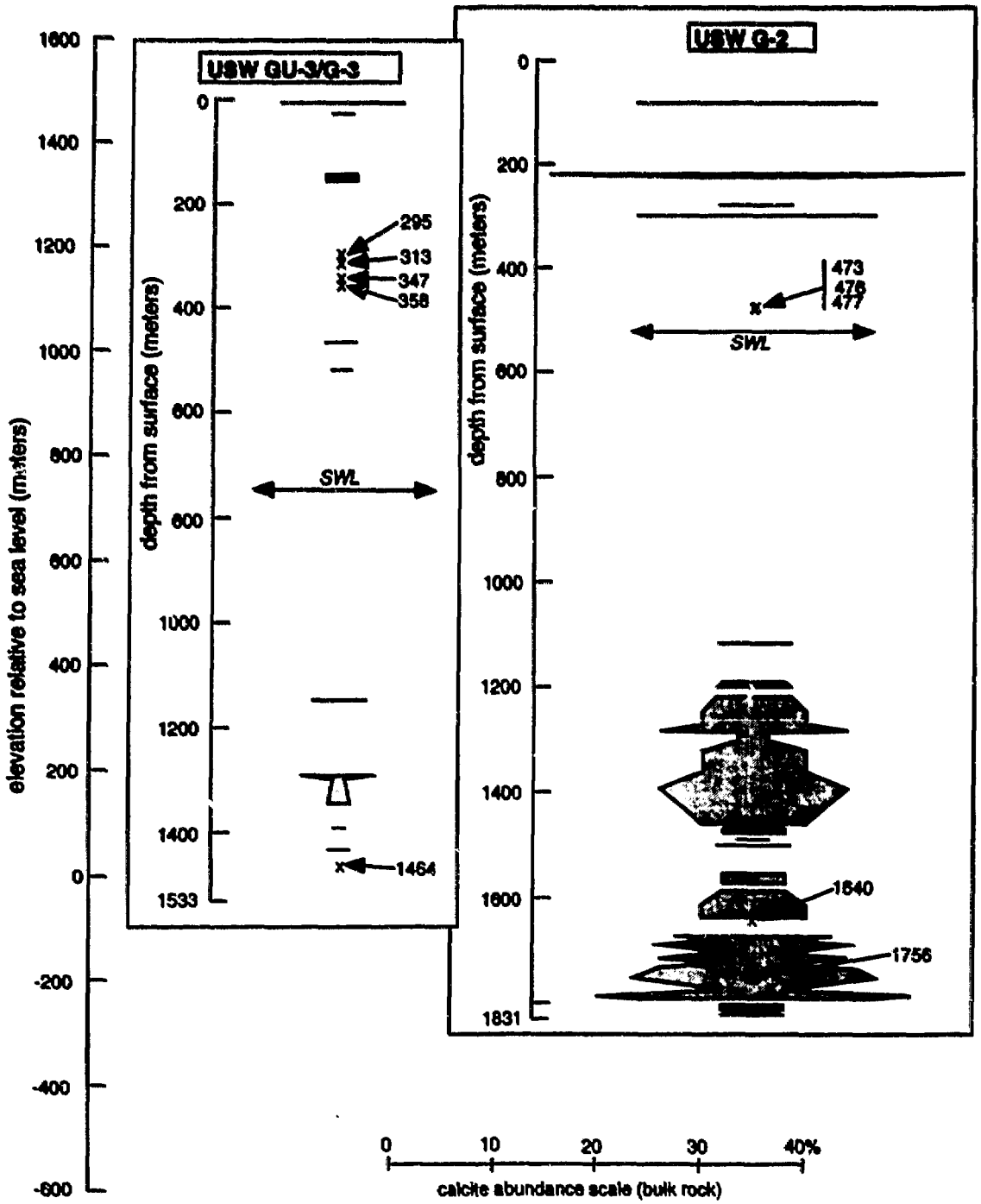

Fig. 1: Locations of fracture-calcite samples (x) within drill cores USW G-2 and USW GU-3/G-3. The numbers used for each sample refer to the sample depth in meters within their respective drill cores. Also shown in this figure are the abundances of calcite within the bulk rock, represented by horizontal lines in discrete occurrences and by stippled patterns in thicker calcite-rich intervals; the percentage of bulk-rock calcite can be measured against the scale at the bottom of the figure (data from Bish and Chipera, 1989). Horizontal arrows mark the position of the static water level (SWL) in these two drill cores.

average calcite abundance in the bulk rock is 8±7% (Bish and Chipera, 1989). The upper boundary of this calcite-rich zone appears to be equivalent to the upper boundary of an 11-Ma fossil hydrothermal zone beneath Yucca Mountain (Bish, 1989). Much of the calcite in this deep interval occurs within the rock matrix and as pseudomorphs after feldspar phenocrysts (Caporuscio *et al.*, 1982); this, along with the common alteration assemblage of calcite-albite-quartz-barite, strongly indicates formation of the deep calcites in the lower 640 m of USW G-2 by hydrothermal alteration.

Bulk-rock samples from drill core USW GU-3/G-3 contain comparatively little calcite (Fig. 1). A sample within 10 m of the surface in devitrified tuff has 12% calcite, but the underlying nonwelded vitric rocks are mostly calcite-free. Moderate calcite abundances occur at depths beginning about 426 m below the present SWL to the bottom of the drill core (1533 m depth); however, the distribution of calcite in this interval is patchy and averages only 3±9%. These deeper calcites are generally restricted to veinlets within the rock and do not replace feldspar phenocrysts as in USW G-2 (Vaniman *et al.*, 1984). The fossil hydrothermal system that is so prominent in the lower 640 m of USW G-2 is not penetrated by USW GU-3/G-3; it is either absent or occurs at greater depth.

The fracture calcites studied for this report were selected from (1) zones that are near the potential repository location above the SWL and (2) deeper fractures beneath the SWL. Fractures containing calcite are generally open above the SWL; fractures below the SWL that were sampled for this report are sealed by calcite. Selection of samples from above and below the SWL in two drill cores provides for a preliminary comparison of major differences between fracture calcites from unsaturated and saturated environments, as well as a comparison of unsaturated-zone calcites in two different drill cores.

Methods

Mineral separates of fracture calcite were hand-picked. These separates were carefully examined under binocular and petrographic microscopes to remove contamination by other minerals, providing clean calcite concentrations of 63 to 139 mg. Clean calcite separates were obtained for all samples except USW G-2 at 1756 m depth; this sample contains finely intergrown quartz that could not be entirely removed. Since X-ray diffraction analysis shows that quartz constitutes only ~5% of this sample and quartz is not a serious chemical contaminant, the chemical data from this separate are considered acceptable for the purposes of this report. Polished thin sections were also prepared from each of the fracture samples. The hand-picked separates were submitted with blind standards to the trace-element geochemistry laboratory at Washington University, Missouri, for instrumental neutron activation analysis (INAA); the techniques used are described by Korotev (1991). The thin sections were examined petrographically; major- and minor-element calcite compositions were determined using a Cameca MBX electron microprobe operated at 15 kV with a sample current of 15 nA on thorium oxide. Carbonate mineral standards were used for calibration of Ca, Mg, Mn, and Fe; CO_2 was estimated by difference. Examination of energy-dispersive X-ray spectra indicated no other elements present in abundances suitable for electron microprobe analysis. Several thin sections were also examined with an ISI DS-130 scanning electron microscope to obtain backscattered-electron and energy-dispersive chemical imaging.

In the text and figures, each sample is identified by drill core and a number corresponding to its depth in meters from the surface (corresponding to the sample numbers in Fig. 1). In the appendices, cross-reference is also given to the identification numbers used at Los Alamos (LANL numbers)

and in parallel isotopic studies at the U. S. Geological Survey (HD numbers). Electron microprobe data, INAA data, and photomicrographs (semi-crossed polarizers) with brief petrographic descriptions for the fracture calcites are compiled in the appendices. Cation formulae are listed beneath the weight-percent oxide data for the electron microprobe analyses. The INAA data are listed in µg/g for most elements, except for CaO (listed as weight percent oxide) and Au (listed in ng/g). Estimates of analytical precision are given in parentheses (one standard deviation) for all data in the appendices.

Results

Data from fracture calcites in USW G-2

The five fracture calcites analyzed from USW G-2 represent (a) open fractures within the lower devitrified Topopah Spring Member at 473-477 m depth, (b) a closed fracture within an albite- and calcite-altered quartz-latite lava at 1640 m depth, and (c) a closed fracture in an albite-, calcite-, and chlorite-altered dacitic lava/flow breccia at 1756 m depth (Fig. 1). Chemical data and thin-section images of these samples are given in appendices 1 to 5.

Thick calcite coatings on two of the three fractures within the unsaturated zone provided enough material to analyze both earlier- and later-formed calcites. In the sample at 476 m depth, a 5-8 mm thick layer of equant rhombohedral calcite is overlain by small (<1 mm) pyramidal prismatic calcites (photomicrograph in Appendix 2). These earlier and later forms were sampled separately. Chemical data for these two different forms indicate a 7 to 10x increase in light rare-earth elements (LREE, La-Nd) and 5x increase in heavy rare-earth elements (HREE, Tb-Lu) in late vs. early calcite; Sc and Fe are also enriched by a factor of 2x, and Th by 10x in the later calcite.

The nearby sample at 477 m depth was also thick enough (5 mm) to permit sampling of both early and late calcites, but here all calcite occurs as massive acute-rhombohedral or scalenohedral forms (photomicrograph in Appendix 3). In this occurrence, there is a fairly general increase of ~2 to 3x in all rare-earth elements (REE) as well as Sc and Fe. However, there is a decrease of the same magnitude in Rb, Sr, Cs, and U. Uranium and Th appear to be decoupled, because Th increases by 9x in the later-formed pyramidal calcite grains whereas U decreases.

More significant distinctions separate the fracture calcites of the unsaturated zone from those of the saturated zone. Some transition metals are much higher in the deeper calcites (e.g., Sc contents of 0.5-6 µg/g in the saturated-zone calcites vs. <0.02 µg/g in the unsaturated zone; Fig. 2). Two of the deeper calcites have Fe+Sc contents closer to and Fe/Sc ratios similar to the local tuffs. A third (USW G-2 at 1640 m, in the quartz-latite lava) has a relatively low Fe content. This calcite is intergrown with a small amount (<5%) of dolomite (Appendix 4). The enrichment in transition metals is most notable in MnO, which is measurable by electron microprobe at 0.25 to 2.1% in the deeper calcites but is <0.05% in the shallower calcites. In USW G-2, strontium is also considerably higher in the deeper calcites (247-830 mg/g, vs. 11-94 mg/g in the shallower calcites).

In addition to these differences in element abundances, the relative abundances of the REE are markedly different in calcites above and below the SWL (Fig. 3). The development of strong negative Eu and Ce anomalies in calcites above the SWL distinguishes these calcites from those below the SWL.

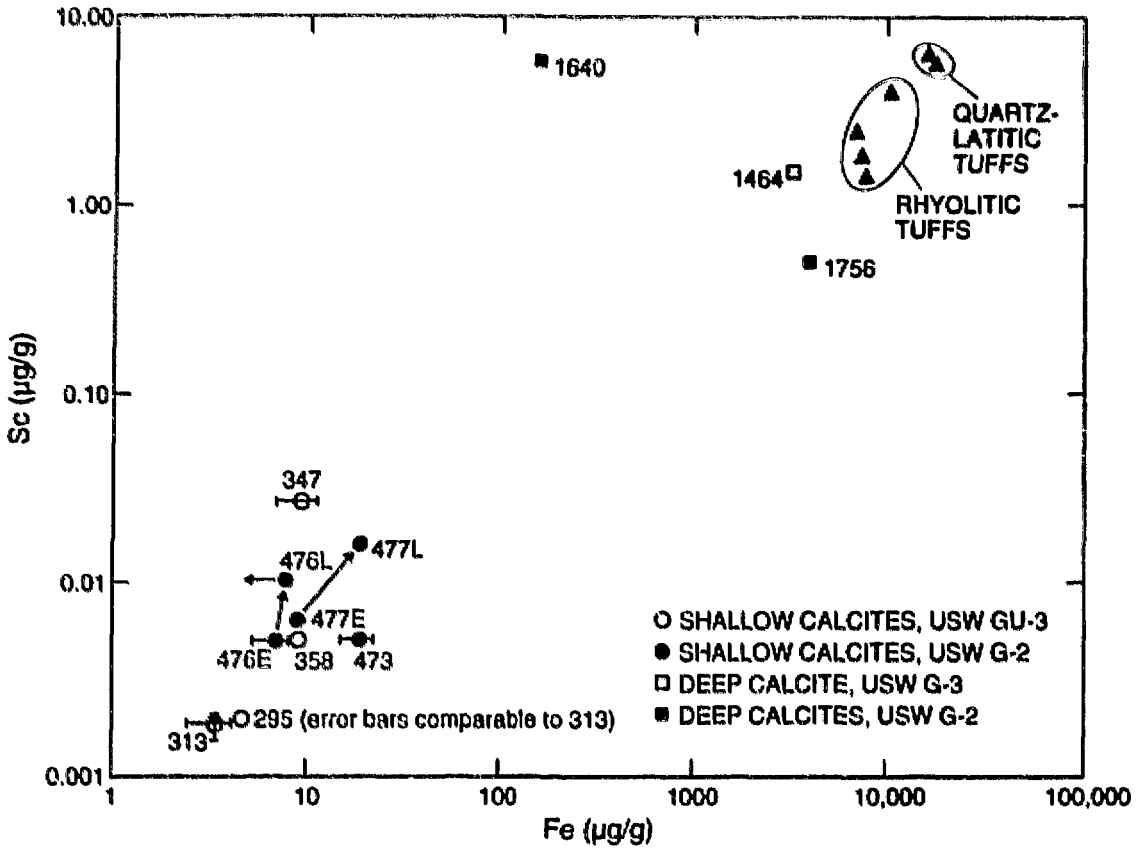

Fig. 2: Log-scale plot of Sc and Fe abundances (INAA data) in fracture calcites. The Fe value for USW G-2 476L is the maximum that this calcite might contain; Fe in this sample is below detection limits, as indicated by the arrow pointing to lower Fe values. These data are compared to literature data for local tuff units (Broxton *et al.*, 1989). Deeper calcites, below the SWL, have considerably higher Fe and Sc contents than shallow calcites. Labels E and L indicate early-formed and late-formed calcite within a single fracture. Representative error bars (± 1 standard deviation) for Fe are shown for several of the shallow calcites; error bars for the deep calcites are smaller than the symbols used. Error bars for Sc are smaller than the symbols used, except for USW GU-3 295 and 313.

Data from fracture calcites in USW GU-3/G-3

Fracture calcites analyzed from USW GU-3/G-3 represent (a) open fractures within the lower devitrified Topopah Spring Member at 295-358 m depth and (b) a closed fracture in the analcime-altered lower part of the Lithic Ridge Tuff at 1464 m depth. Chemical data and thin-section images of these samples are given in Appendices 6 to 10.

Subsplits of early-formed and late-formed calcite were not sampled within individual fractures in USW GU-3/G-3; therefore, the variation of calcite composition in successive generations can not be evaluated for the unsaturated-zone calcites of this core as they were for USW G-2. However, many of the distinctive differences between calcite above and below the SWL are similar to those observed in USW G-2. Transition-metal concentrations in the deeper calcite are much higher than in calcites above the SWL (1.55 µg/g Sc vs. 0.003 µg/g or less; 3190 µg/g Fe vs. <10 µg/g; Fig. 2). As in USW G-2, the elevated concentrations of transition metals are readily observed in electron

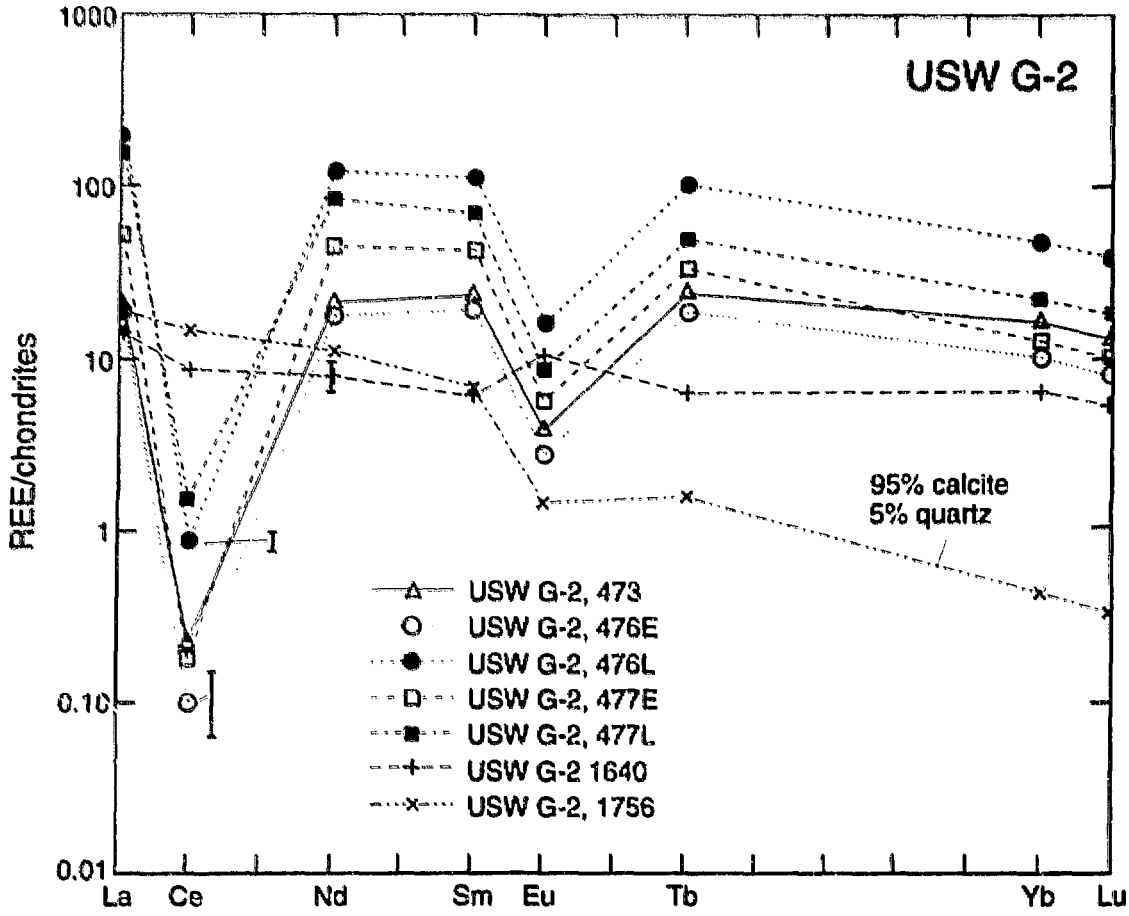

Fig. 3: Chondrite-normalized abundances of rare-earth elements (REE) in fracture calcites from USW G-2. Chondritic values used for normalization (μg/g) are La(0.33), Ce(0.88), Nd(0.6), Sm(0.181), Eu(0.069), Tb(0.047), Yb(0.2), and Lu(0.034). Notable in this figure are the generally high contents of REE in the shallow calcites and their prominent negative Ce and Eu anomalies, contrasted with the absence of such anomalies in calcites from greater depth (1640 and 1756 m). Labels E and L indicate early-formed and late-formed calcite within a single fracture. Representative error bars (± 1 standard deviation) are shown for Ce in USW G-2 476E and 476L, as well as for Nd in G-2 1640. For La, Sm, Eu, Tb, Yb, and Lu, as well as the highest Nd concentrations, error bars are smaller than or only slightly larger than the symbols used.

microprobe analyses that reveal measurable MnO contents in the deeper calcite (4.7-5.8%), contrasted with calcites above the SWL that contain <0.1% MnO.

Figures 3 and 4 show that the large negative Eu and Ce anomalies in chondrite-normalized REE patterns of calcites above the SWL are characteristic in both USW G-2 and USW GU-3/G-3. The deepest calcites from below the SWL in both drill cores lack these large negative anomalies, although work in progress indicates that calcites from relatively shallow depths beneath the SWL in USW GU-3/G-3 can have prominent negative Ce anomalies. There is significant chemical variability in calcites from above the SWL. Strontium values in the calcites above the SWL range from below detection limits (<12 μg/g) to 338 μg/g. For the samples above the SWL described in this report, the concentrations of REE range over two orders of magnitude. The data shown here suggest an apparently lower REE content in calcites above the SWL from USW GU-3/G-3 than in comparable

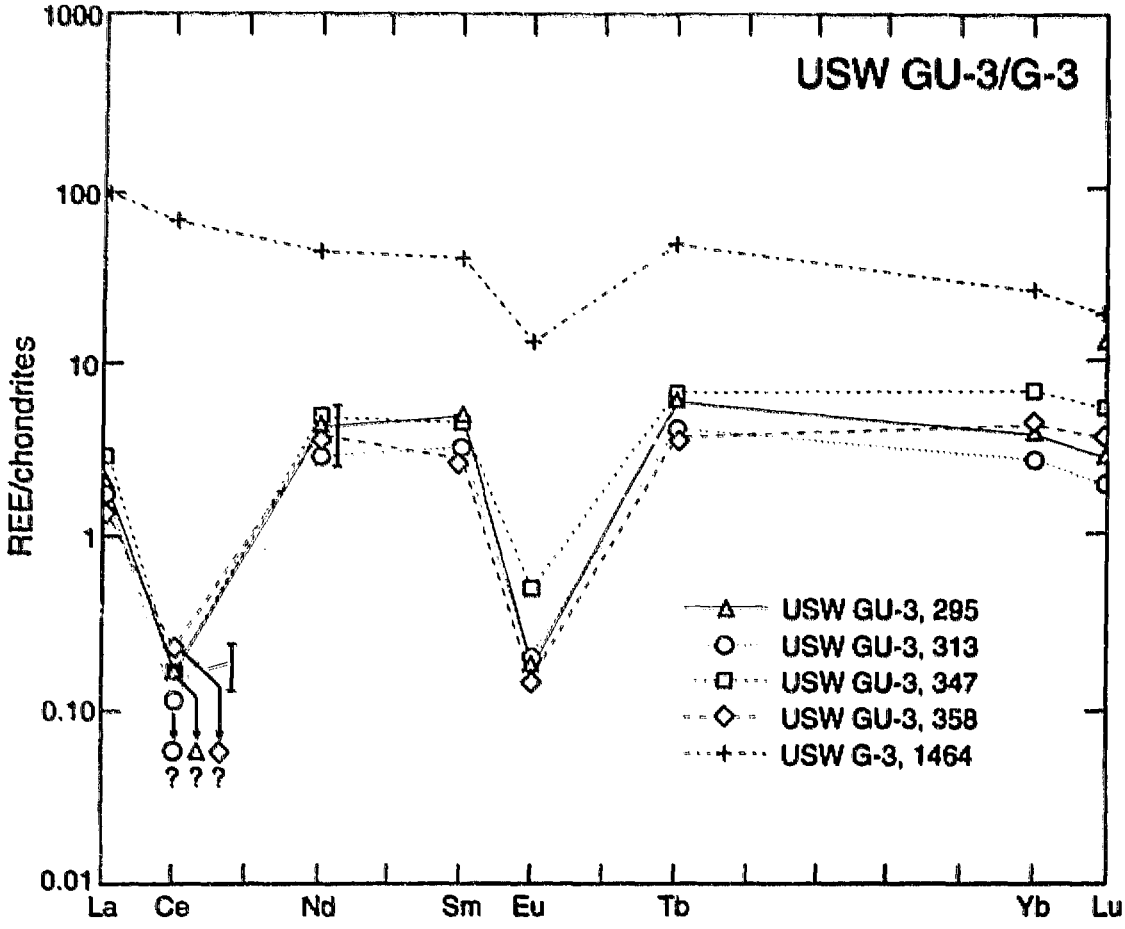

Fig. 4: Chondrite-normalized abundances of rare-earth elements (REE) in fracture calcites from USW GU-3/G-3, using normalization values listed in Fig. 3. As in Fig. 3, the negative Ce and Eu anomalies of the shallow calcites contrast with the presence of only a slight Eu anomaly in the deeper calcite (1464 m depth). Many Ce values in the shallow calcites of USW GU-3/G-3 are below detection limits (0.1-0.2 μg/g), leading to the "bottomless" Ce anomalies indicated here for samples at 295, 313, and 358 m depth. Error bars (± 1 standard deviation) are shown for Ce in USW GU-3 347 and Nd in GU-3 358 (representative of other Nd errors in calcites with similar Nd concentration). For all other data, including Nd in G-3 1464, error bars are smaller than or only slightly larger than the symbols used.

calcites in USW G-2, but work now in progress indicates a very broad range of overlapping REE concentrations. The range of Sr contents may be just as large.

Discussion

Differences in calcite chemistry above and below the SWL

The chemical and petrographic data for fracture calcites from cores USW G-2 and USW GU-3/G-3 indicate significant differences between calcites above and below the SWL. At present there are not enough data to indicate whether the position of the SWL is an operative factor in determining

the type of calcite deposited, but for the time being the SWL serves as a useful reference horizon. The data of Whelan and Stuckless (1992) and of Peterman *et al.* (1992) suggest that past changes in position of the SWL might be tracked by variations in calcite stable- or radiogenic-isotope compositions; if so, then the corresponding trace- and minor-element compositions of calcites may prove to be another indicator of saturated or unsaturated depositional environment.

Fracture calcites that formed at depths well below the SWL have chondrite-normalized REE patterns that lack any Ce anomaly; they also contain relatively large amounts of some transition metals, detectable by INAA analysis (Fe, Sc) or electron microprobe analysis (Mn). Fracture calcites from above the present SWL contain only small amounts of the transition metals and generally have chondrite-normalized REE patterns with large negative Eu and Ce anomalies. The data available for calcites from USW G-1 support this conclusion, although two anomalous calcites have been found in USW G-4 (Vaniman, 1993). In USW G-4, one calcite from 433 m above the SWL lacks a negative Eu anomaly and one calcite 270 m below the SWL has the large negative Ce and Eu anomalies that are characteristic of the unsaturated zone. All of the calcites in USW G-4, including the one that is 270 m below the present SWL, have low concentrations of transition metals typical of calcites that form above the SWL. Work in progress indicates that the general distinctions in REE and transition-metal character noted here for calcites above and below the present SWL holds true for most calcites from Yucca Mountain, but exceptions continue to be found. These exceptions to the otherwise general distinctions between saturated-zone and unsaturated-zone calcites indicate that much information about paleohydrology is recorded in the chemistry of calcite deposits.

Variability in shallow-calcite compositions

The prominent negative Ce and Eu anomalies that are generally typical of shallow calcites suggest that most calcites above the SWL are, as a group, distinct from calcites below the SWL. The general similarity in chondrite-normalized REE patterns suggests common Eu and Ce fractionation processes in the origins of shallow calcites of both drill cores. A more detailed consideration of the Ce and Eu anomalies, however, shows that there is significant variability among the shallow calcites in the magnitude of the Eu anomaly and perhaps in the magnitude of the Ce anomaly. Figure 5 plots the depth of the Eu anomaly (measured by dividing chondrite-normalized Eu concentration into the chondrite-normalized concentration of the next-lightest lanthanide, Sm) against the depth of the Ce anomaly (similarly measured as chondrite-normalized La/Ce). A quantitative assessment of the Ce anomaly is hampered by the fact that Ce contents are so low that they are beneath detection limits in three of the four calcites analyzed from USW GU-3/G-3. Nevertheless, the data are sufficient to show great variability in both the Eu and Ce anomalies.

Most lanthanide elements are trivalent; however, Ce may be depleted by precipitation as Ce^{IV} (CeO_2) from waters that are oxidizing or of high pH (Fig. 6A). The well-studied coprecipitation of Ce^{IV} with Mn^{IV} in oceanic manganese nodules (Brookins, 1989) may be relevant to the formation of unsaturated-zone calcites in fractures at Yucca Mountain, where Mn^{IV} manganese minerals (lithiophorite and rancieite) are common in unsaturated-zone fractures. Carlos *et al.* (1993) note that rancieite in fractures at Yucca Mountain may contain as much as 8% CeO_2 by weight. If the fluids from which these shallow calcites have formed were modified by manganese-mineral precipitation and if many of these calcites are as young as the data of Szabo and Kyser (1990) suggest, then the formation of Mn-oxides as well as calcite may be an ongoing process at Yucca Mountain. Alternatively, Ce^{IV} may be actively scavenged from calcite-forming waters by Mn-

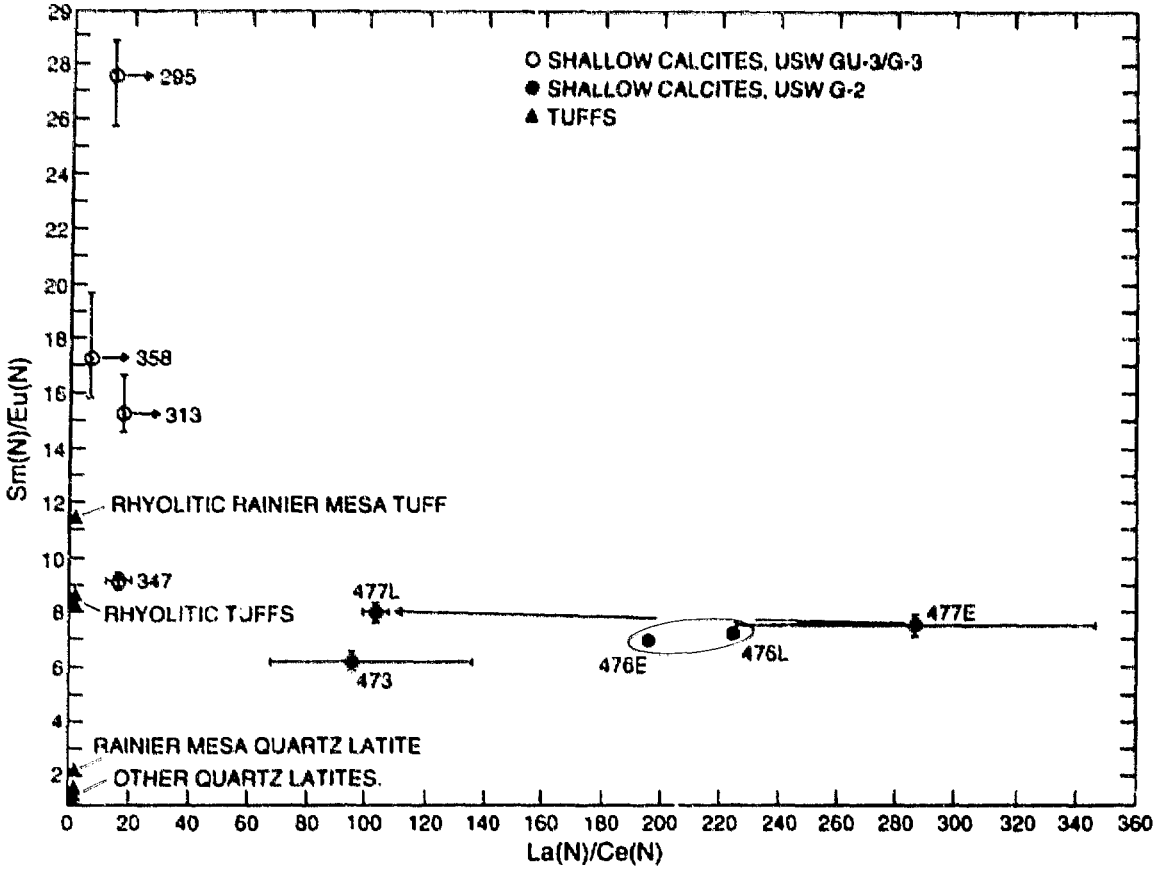

Fig. 5: Comparison of relative measures of the depth of the Ce and Eu anomalies in shallow fracture-calcites of USW G-2 and USW GU-3/G-3. Chondrite-normalized values are used for La(N), Ce(N), Sm(N), and Eu(N); in general, higher La(N)/Ce(N) indicates a deeper negative Ce anomaly and higher Sm(N)/Eu(N) indicates a deeper negative Eu anomaly, although these values are affected secondarily by the slope of the REE pattern (Figs. 3, 4). For the samples from USW G-2, early (E) and late (L) deposits within a single fracture lining are compared; the subsamples USW G-2 476E and 476L are close enough that the difference in their La(N)/Ce(N) is not significant. This figure illustrates the generally greater depth of the negative Eu anomaly (higher position on the vertical axis) in shallow calcites of USW GU-3/G-3, contrasted with the lesser Eu anomalies of shallow calcites in USW G-2. The Sm/Eu ratio in the shallow calcites of USW G-2 is the same as that in the host rhyolitic tuffs (tuff data from Broxton *et al.*, 1989). Negative Ce anomalies are greater in the calcites of USW G-2 than in USW GU-3/G-3 347; however, the depth of the Ce anomaly in the other three samples from USW GU-3/G-3 (295, 313, and 358) may be greater than shown here because Ce is below detection limits in these samples. Representative error bars are shown, based on one-standard-deviation limits for (maximum numerator)/(minimum denominator) and (minimum numerator)/(maximum denominator).

oxides that have already formed. A third possibility is that most of the calcites yet analyzed for trace elements are very old, and were formed along with Mn oxides soon after tuff emplacement. This last possibility is considered unlikely.

In contrast to the negative Ce anomalies attributed to Ce oxidation, negative Eu anomalies are typically attributed to Eu reduction, from Eu^{III} to Eu^{II} (Fig. 6B). In divalent form, Eu readily substitutes for Ca and Sr in many common minerals, including calcite. In the igneous processes that formed the various siliceous magmas beneath Yucca Mountain, Eu and Sr are roughly correlated (Fig. 7). In contrast, the aqueous processes of calcite precipitation above the SWL have formed

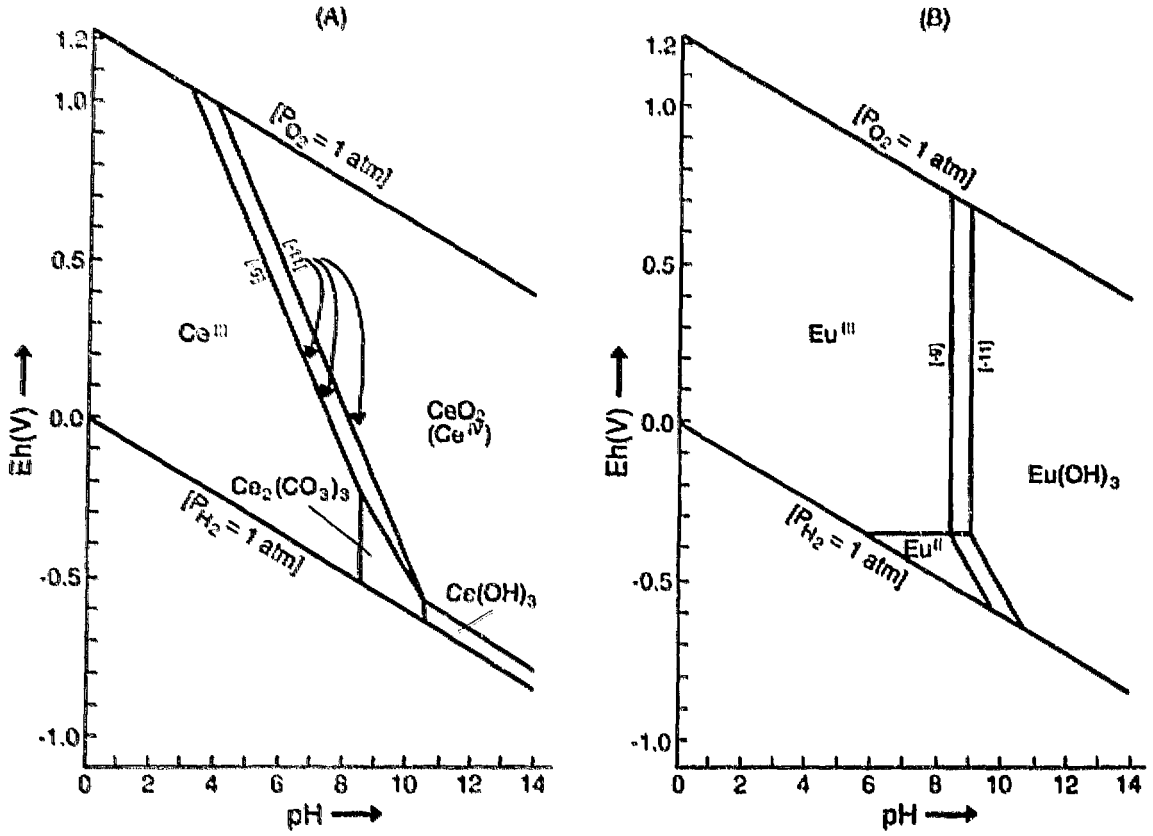

Fig 6: Eh-pH diagrams for Ce and Eu, after Brookins (1989), for parts of the system Ce-C-O-H with activity of total dissolved CO_3=10^{-3} (Fig. 6A) and for the system Eu-O-H (Fig. 6B). Both figures are for 25°C and 1 atm total pressure. Curves for dissolved activities of the relevant lanthanides at 10^{-9} and 10^{-11} are shown. Note that the stability field of Ce^{IV} (CeO_2) expands with increased Ce concentration (e.g., evaporation). Eu fractionation as Eu^{II} is limited to reducing solutions, whereas Ce fractionation as Ce^{IV} is favored by oxidizing solutions. Some possible Eh-pH water evolution paths are shown in 6A, beginning with oxidizing soil waters that rise in pH with evaporative concentration and are modified with depth into more neutral and less oxidizing compositions (hypothetical paths based on Kerrisk, 1987 and Vaniman *et al.*, 1992).

contrasting high-Sr calcites (in most of USW GU-3) or high-Eu calcites (in most of USW G-2; see Fig. 7). Moreover, the Eu anomalies of most shallow calcites in USW GU-3 exceed those of the local tuffs (Fig. 5).

It is possible that the exceptionally low Eu contents of shallow calcites of USW GU-3/G-3 may be caused by scavenging of Eu by another Ca-rich mineral. In USW GU-3 fluorite (CaF_2) commonly occurs beneath the calcites above the SWL (see Appendices 6, 7, and 8). Early precipitation of fluorite could deplete Eu from waters that later precipitated calcite, but fluorite analyzed from the same fracture as USW GU-3 295 has the same magnitude of negative Eu anomaly as the texturally overlying calcite (work in progress). Fluorite therefore appears not to have concentrated Eu from solutions that later precipitated calcite. Ca-zeolites (probably heulandite or stellerite) are intergrown with the calcite at 477 m in USW G-2 (see Fig. 8 and Appendix 3). The calcite of this sample is deposited over small, blocky crystals of Ca-zeolite. The outermost portions of the calcite also contain anhedral inclusions of Ca-zeolite that formed along grain boundaries (z1 in Fig. 8), and the exterior surfaces and fractures in the calcite are locally covered or filled by small

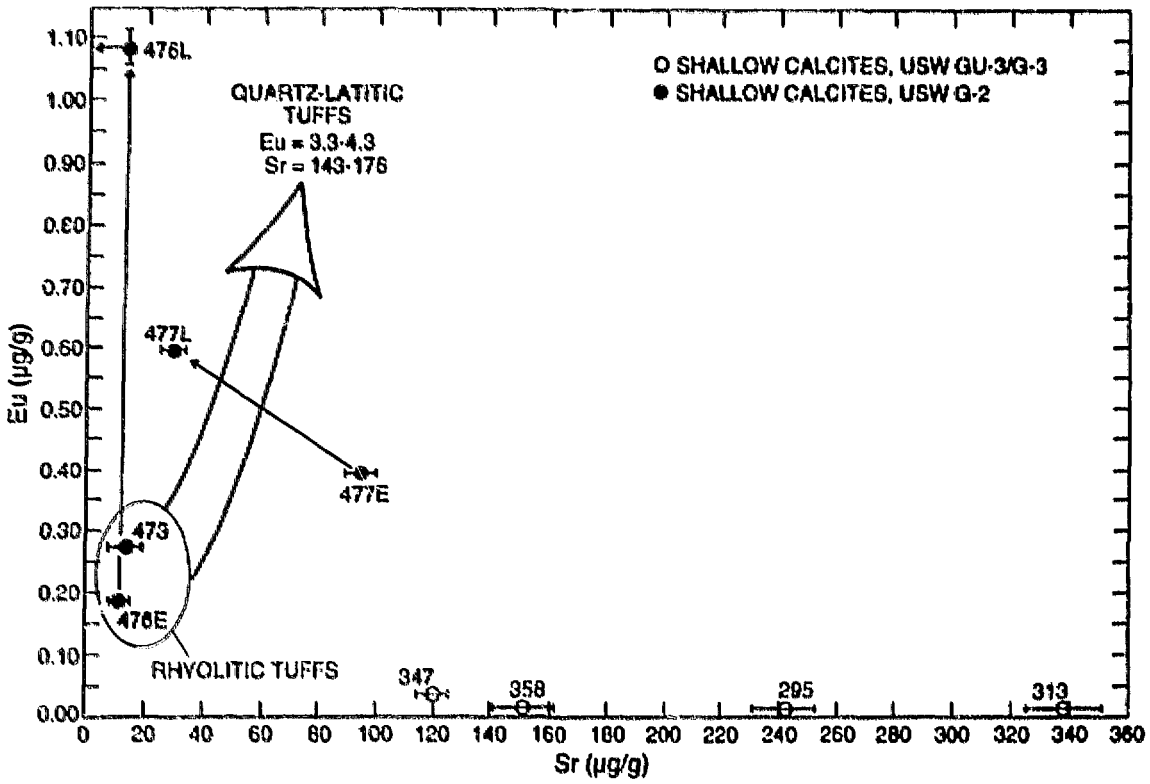

Fig. 7: Plot of Eu vs. Sr for shallow calcites in USW G-2 and USW GU-3/G-3. Strontium contents of the shallow calcites in USW GU-3/G-3 are significantly higher than in shallow calcites of USW G-2, suggesting deposition from Sr-enriched fluids. Strontium and Eu contents are not correlated in either set of calcites. The data for tuff samples are from Broxton *et al.* (1989). Labels E and L indicate early-formed and late-formed calcite within a single fracture. Error bars (± 1 standard deviation) are shown for Sr; the Sr value shown for the USW G-2 476L is a maximum, as indicated by the small arrow pointing toward the y axis. Error bars for Eu are smaller than the symbols used except in USW G-2 476L. For comparison, the compositions of rhyolitic tuffs (shaded oval) and quartz-latitic tuffs (with Eu off-scale in direction of the broad arrow) would define calcite Eu/Sr ratios unlike any of the shallow GU-3/G-3 calcites.

Ca-zeolite crystals (z2 in Fig. 8). Textural evidence supports the formation of Ca-zeolite before, along with, and after calcite precipitation in USW G-2. It is possible that zeolites such as this precipitated separately from calcite in USW GU-3 and may have removed significantly more Eu from solution, but this explanation will have to be tested by analyses of fracture zeolites. Most importantly, any mechanism that would segregate Eu from the other lanthanides during calcite precipitation would require reducing conditions (Fig. 6B), whereas all episodes of late-stage crystallization and precipitation in the tuffs of Yucca Mountain appear to have been events of relatively high Eh (Vaniman *et al.*, 1984). Experimental studies suggest little fractionation of REE during calcite precipitation from dilute solutions (Terakado and Masuda, 1988).

If the Eu anomalies in calcites did not develop during precipitation, they may have been inherited from the source rocks for the calcite-forming fluids. The data from local tuffs plotted in Fig. 5 suggest that all of the shallow calcites analyzed from USW G-2 and the sample USW GU-3 347 may have inherited Eu anomalies comparable to those of the rhyolitic tuffs. Congruent dissolution of tuff — either from fracture walls or from detritus in overlying soils — is conceivable for the generation of the Eu anomalies in these calcites. The greater Eu anomalies in some of the shallow

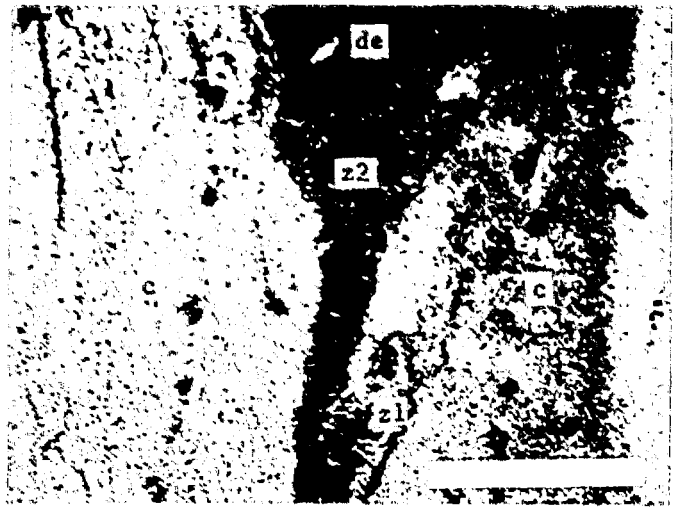

Fig. 8: Ca-zeolite (z1) intergrown with calcite (c) and deposited in an open fissure between calcite crystals (z2) in USW G-2 477. The open surface of the fracture is toward the top of this photomicrograph. Fine-grained tuff and calcite detritus (de) fill in the secondary fracture above z2. Scale bar is 0.3 mm.

calcites of USW GU-3 samples (295, 313, and 358; Fig. 5) may arise if other rock types are involved (e.g., leaching of eolian sources in surface soils) or if dissolution is incongruent, favoring minerals with deeper Eu anomalies in forming the solutions from which the calcites with deep Eu anomalies have precipitated. Although incongruent dissolution of soil constituents is likely to be a factor in determining the nature of surface waters, it is important to note that the behavior of lanthanides during weathering is poorly understood (Brookins, 1989).

In contrast to the requirement for reducing conditions, other source rocks, or incongruent dissolution to account for deep Eu anomalies, the formation of Ce anomalies may directly reflect the oxidizing conditions of shallow-calcite precipitation. Evaporative concentration of soil waters can enhance the segregation of Ce as Ce^{IV} (Fig. 6A). Oxidized waters can allow ongoing formation of negative Ce anomalies in calcite by precipitation or sorption of Ce^{IV} onto other minerals (such as Mn-oxides) that occur on fracture surfaces. This hypothesis can be tested by analysis of these minerals to seek complementary positive Ce anomalies.

Conclusions

Chemical data from the fracture calcites in USW G-2 and USW GU-3/G-3 provide evidence that (1) shallow fracture calcites, above the SWL, were formed in an environment generally distinct from that in which deeper calcites formed and that (2) the shallow fracture calcites, while more closely related to each other than to the deeper calcites, are also highly variable in composition. The underlying cause of the distinction between deep and shallow calcites may be attributable to formation of the deep calcites from waters of the Paleozoic aquifer (Peterman *et al.*, 1992), with at least some deposition during ancient hydrothermal events (Bish, 1989), whereas the shallow calcites arise from separate processes that probably involve surface-derived waters. However, both the isotopic data and the chemical data leave open the possibility that some of the shallow calcites may

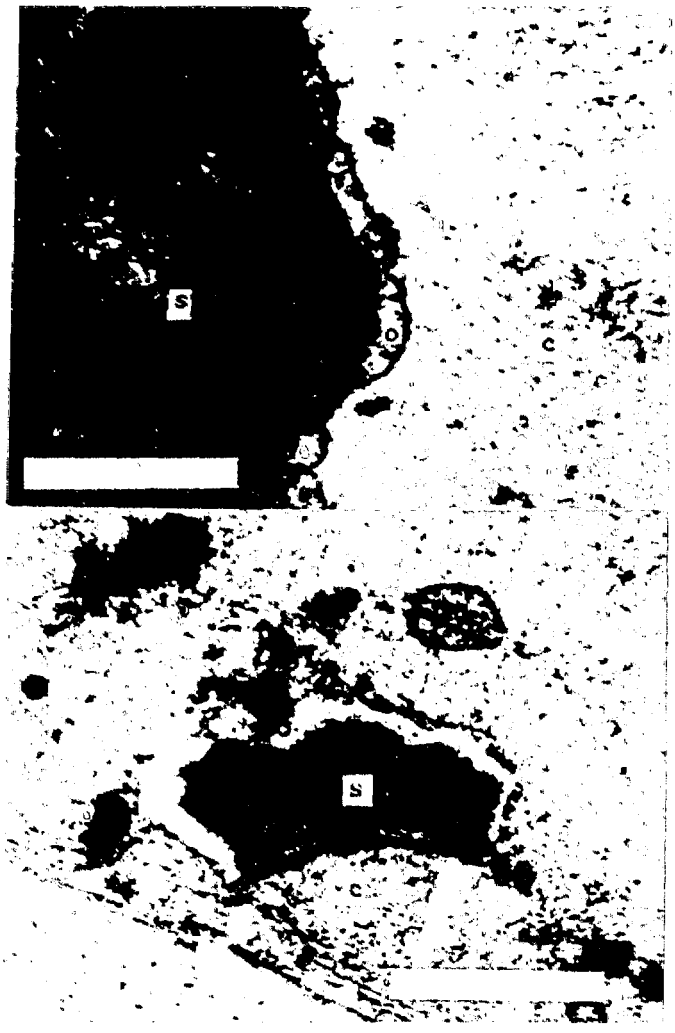

Fig. 9: Sepiolite (s) and opal (o) associated with calcite (c) in USW GU-3/G-3 295. Scale bars are 0.3 mm.

be quite old, formed from aqueous fluids soon after tuff devitrification. The causes of variability in the shallow calcites of these two drill cores may reflect competition with other minerals for certain trace elements during calcite precipitation, incongruent dissolution of source rocks in the origins of calcite-forming fluids, and perhaps other processes not evident in the limited data that have been collected so far.

It is important to emphasize that the data presented here represent only a small set of fracture calcites, and include none of the matrix calcites that are more abundant in some portions of these two drill cores (Fig. 1). These matrix calcites may be closely related to the nearby fracture calcites and possess similar properties, but at present the relations between them are unknown. If much of the fracture calcite is relatively young and if the fracture calcites above the SWL are largely derived from surface sources, then the chemical systematics of soil-zone calcite formation may provide important clues to the origins of fracture calcites deposited above the SWL. The calcites in caliche have high Sr contents; although clean separates of the caliche calcites have proven difficult to

obtain, INAA analyses of calcite-opal and caclite-sepiolite separates from the caliche allow estimation of 800-2100 µg/g Sr in these calcites (Vaniman *et al.*, in press). The high Sr contents in calcites above the SWL in USW GU-3/G-3 (Fig. 7) may be related to the high Sr contents of caliche.

Both opal and the chain-structure clay sepiolite are important associates of the calcite that forms in caliche at the surface of Yucca Mountain (Vaniman *et al.*, 1992; Vaniman *et al.*, in press). Fracture calcites in USW GU-3 at 295 m (appendix 6) also contain small masses of sepiolite, with opal concentrated at the contact between sepiolite and calcite (Fig. 9A). This texture is somewhat ambiguous, since it may be explained by simultaneous precipitation, by replacement of earlier calcite, or by precipitation of later calcite around the sepiolite masses. Elsewhere in the same sample, sepiolite appears to have formed in layers within voids, parallel to the void walls within previously-formed calcite (Fig. 9B). The occurrence of sepiolite as well as opal in shallow fracture calcites is a further indication of the possible linkage between soil mineralogy and the minerals precipitating along fracture surfaces above the static water level at Yucca Mountain.

Acknowledgements

This work was supported by the Yucca Mountain Site Characterization Project as part of the Civilian Radioactive Waste Management Program. This Project is managed by the U. S. Department of Energy, Yucca Mountain Site Characterization Project. Review comments by B. Carlos are greatly appreciated. The Yucca Mountain Project Technical Data Catalog Data Tracking Number for this paper is LA0000000000014.002.

References

Bish D. L. (1989) Evaluation of past and future alterations in tuff at Yucca Mountain, Nevada, based on the clay mineralogy of drill cores USW G-1, G-2, and G-3. *Los Alamos Nat. Lab. Rept. LA-10667-MS*, 40 pp. NNA.890126.0207

Bish D. L. and S. J. Chipera (1989) Revised mineralogic summary of Yucca Mountain, Nevada. *Los Alamos Nat. Lab. Rept. LA-11497-MS*, 68 pp. NNA.891019.0029

Brookins D. G. (1989) Aqueous geochemistry of rare earth elements. In *Geochemistry and Mineralogy of Rare Earth Elements* (B. R. Lipin and G. A. McKay, eds.), Min. Soc. of Amer. Rev. in. Mineralogy, Vol. 21, 201-225. NNA.931028.003

Broxton D. E., R. G. Warren, and F. M. Byers (1989) Chemical and mineralogic trends within the Timber Mountain — Oasis Valley caldera complex, Nevada: Evidence for multiple cycles of chemical evolution in a long-lived silicic magma system. *Jour. Geophys. Res.* 94, 5961-5985. NNA.920319.0004

Caporuscio F., D. Vaniman, D. Bish, D. Broxton, B. Arney, G. Heiken, F. Byers, R. Gooley, and E. Semarge (1982) Petrologic studies of drill cores USW G-2 and UE25b-1H, Yucca Mountain, Nevada. *Los Alamos Nat. Lab. Rept. LA-9255-MS*, 111 pp. NNA.870519.0041

Carlos B. A. (1987) Minerals in fractures of the saturated zone from drill core USW G-4, Yucca Mountain, Nye County, Nevada. *Los Alamos Nat. Lab. Rept. LA-10927-MS*, 32 pp. NNA.870708.0026

Carlos B. A., S. J. Chipera, D. L. Bish, and S. J. Craven (1993) Fracture-lining manganese oxide minerals in silicic tuff, Yucca Mountain, Nevada, U.S.A. *Chem. Geol.* 107, 47-69. NNA.931028.0002

Kerrisk J. F. (1987) Groundwater chemistry at Yucca Mountain, Nevada, and vicinity. *Los Alamos Nat. Lab. Rept. LA-10929-MS*, 118 pp. NNA.870507.0017

Korotev R. L. (1991) Geochemical stratigraphy of two regolith cores from the central highlands of the Moon. *Proc. 21st Lunar Planet. Sci. Conf. (V. L. Sharpton and G. Ryder, eds.). Lunar and Planetary Inst., Houston*, 229-289. NNA.921019.0162

Norris A. E., F. M. Byers, Jr., and T. J. Merson (1986) Fran Ridge horizontal coring summary report, hole UE-25h#1, Yucca Mountain area, Nye County, Nevada. *Los Alamos Nat. Lab. Rept. LA-10859-MS*, 78 pp. NNA.891129.0072

Peterman Z. E., J. S. Stuckless, B. D. Marshall, S. A. Mahan, and K. Futa (1992) Strontium isotope geochemistry of calcite fracture fillings in deep core, Yucca Mountain, Nevada — a progress report. In *High Level Radioactive Waste Management*, Amer. Soc. Civil Eng. and Amer. Nuc. Soc., Proc. 3rd Internat. Conf., Las Vegas, Nevada, 1582-1586. NNA.921116.0073

Szabo B. J. and T. K. Kyser (1990) Ages and stable-isotope compositions of secondary calcite and opal in drill cores from Tertiary volcanic rocks of the Yucca Mountain area, Nevada. *Geol. Soc. Amer. Bull.* 102, 1714-1719. NNA.910225.0068

Terakado Y. and A. Masuda (1988) The coprecipitation of rare-earth elements with calcite and aragonite. *Chem. Geol.* 69, 103-110. NNA.931012.0001

Vaniman D. T. (1993) Calcite deposits in fractures at Yucca Mountain, Nevada. In *High Level Radioactive Waste Management*, Amer. Soc. Civil Eng. and Amer. Nuc. Soc., Proc. 4th Internat. Conf., Las Vegas, Nevada, 1935-1939. NNA.931028.0001

Vaniman D., D. Bish, D. Broxton, F. Byers, G. Heiken, B. Carlos, E. Semarge, F. Caporuscio, and R. Gooley (1984) Variations in authigenic mineralogy and sorptive zeolite abundance at Yucca Mountain, Nevada, based on studies of drill cores USW GU-3 and G-3. *Los Alamos Nat. Lab. Rept. LA-9707-MS*, 71 pp. NNA.870519.0043

Vaniman D. T., S. J. Chipera, and D. L. Bish (in press) Pedogenesis of siliceous calcretes at Yucca Mountain, Nevada. *Geoderma*. (not yet available)

Vaniman D. T., M. H. Ebinger, D. L. Bish, and S. J. Chipera (1992) Precipitation of calcite, dolomite, sepiolite and silica from evaporated carbonate and tuffaceous waters of southern Nevada. In *Water-Rock Interaction 7*, Proc. 7th Internat. Symp. on Water-Rock Interaction, A. A. Balkema, Brookfield, Vermont, 687-691. NNA.930105.0015

Whelan J. F. and J. S. Stuckless (1992) Paleohydrologic implications of the stable isotopic composition of secondary calcite within the tertiary volcanic rocks of Yucca Mountain, Nevada. In *High Level Radioactive Waste Management*, Amer. Soc. Civil Eng. and Amer. Nuc. Soc., Proc. 3rd Internat. Conf., Las Vegas, Nevada, 1572-1581. NNA.930121.0109

APPENDICES: CALCITE PETROGRAPHY AND CHEMISTRY

APPENDIX: CALCITE PETROGRAPHY AND CHEMISTRY - 1

Sample USW G-2, 473 m (LANL-33; HD-273)

electron microprobe analyses:

	cc1	cc3	cc4
CaO	56.5(3)	56.2(3)	56.1(3)
MgO	0.00	0.00	0.00
FeO	0.04(4)	0.05(4)	0.00
MnO	0.01(2)	0.01(2)	0.00
CO_2	43.5	43.7	43.9
Ca	1.014	1.008	1.003
Mg	0.000	0.000	0.000
Fe	0.001	0.001	0.000
Mn	0.000	0.000	0.000
C	0.992	0.998	1.000
Σ	2.007	2.007	2.003

Coarse calcite (c) formed over vapor-phase crystals along a fracture in devitrified tuff. Scale bar is 1 mm.

INAA analysis:

CaO	55.2(8)%
Na	23.2(1.1)µg/g
Sc	0.0051(2)
Cr	<1
Fe	19(2)
Co	0.014(2)
Ni	<5
Zn	4.0(1.0)
As	2.91(6)
Se	- -
Br	<0.11
Rb	<0.6
Sr	14(4)
Zr	<7
Sb	<0.01
Cs	0.023(4)
Ba	<7
La	7.13(10)
Ce	0.20(6)
Nd	13.1(7)
Sm	4.41(6)
Eu	0.274(5)
Tb	1.146(16)
Yb	3.31(5)
Lu	0.455(6)
Hf	<0.02
Ta	<0.004
W	<0.3
Th	0.043(6)
U	0.32(2)
Au	0.6(2)ng/g

APPENDIX: CALCITE PETROGRAPHY AND CHEMISTRY - 2

Sample USW G-2, 476 m (LANL-36; HD-274)

electron microprobe analyses:

	early(cE) cc2	late(cL) cc3	late(cL) cc4
CaO	56.7(3)	56.7(3)	56.6(3)
MgO	0.00	0.00	0.16(2)
FeO	0.01(4)	0.05(4)	0.01(4)
MnO	0.00	0.00	0.00
CO_2	43.3	43.3	43.2
Ca	1.015	1.014	1.018
Mg	0.000	0.000	0.004
Fe	0.000	0.001	0.000
Mn	0.000	0.000	0.000
C	0.983	0.983	0.990
Σ	1.998	1.998	2.012

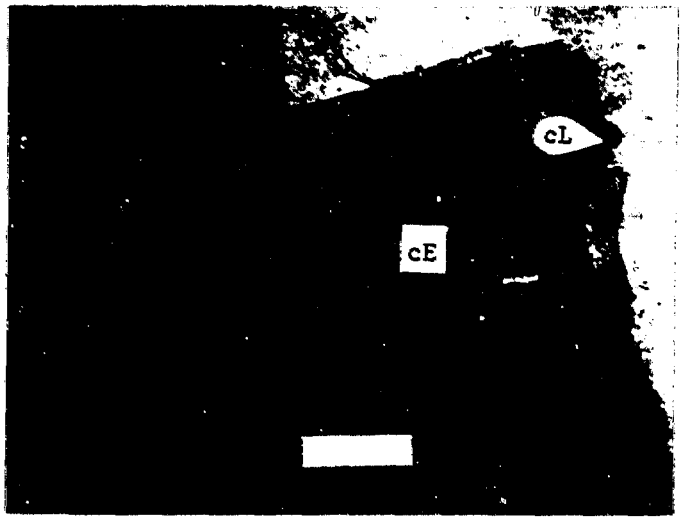

Two generations of calcite along an open fracture; early coarse spar (cE) and later small (<1 mm) pyramidal crystals (cL). Scale bar is 1 mm.

INAA analyses:

	early(cE)	late(cL)
CaO	55.9(9)%	55.2(9)%
Na	21(3)µg/g	<89 µg/g
Sc	0.00494(12)	0.0104(4)
Cr	<1	<2
Fe	7(1)	<8
Co	0.0107(13)	0.004(2)
Ni	<3	<7
Zn	3.0(6)	16(3)
As	0.78(7)	2.1(2)
Se	- -	- -
Br	<0.12	<0.4
Rb	- -	<0.4
Sr	11(3)	<12
Zr	<4	<11
Sb	<0.005	<0.03
Cs	0.138(4)	<0.02
Ba	<7	<15
La	6.59(9)	64.7(9)
Ce	0.09(4)	0.77(5)
Nd	10.8(7)	73(3)
Sm	3.38(5)	20.2(3)
Eu	0.187(3)	1.09(2)
Tb	0.880(12)	4.69(7)
Yb	1.95(3)	9.08(13)
Lu	0.272(4)	1.24(2)
Hf	<0.02	<0.02
Ta	<0.002	<0.01
W	<0.6	<1.2
Th	0.017(3)	0.169(8)
U	<0.1	<0.15
Au	1.5(3)ng/g	1.4(6)ng/g

APPENDIX: CALCITE PETROGRAPHY AND CHEMISTRY - 3

Sample USW G-2, 477 m (LANL-37; HD-275)

electron microprobe analyses:

	early cc1(cE)	early cc2(cE)	late cc3(cL)
CaO	56.4(3)	55.2(3)	55.3(3)
MgO	0.00	0.00	0.00
FeO	0.00	0.00	0.30(5)
MnO	0.00	0.00	0.02(2)
CO_2	43.6	44.8	44.4
Ca	1.012	0.980	0.984
Mg	0.000	0.000	0.000
Fe	0.000	0.000	0.004
Mn	0.000	0.000	0.000
C	0.997	1.013	1.008
Σ	2.009	1.993	1.996

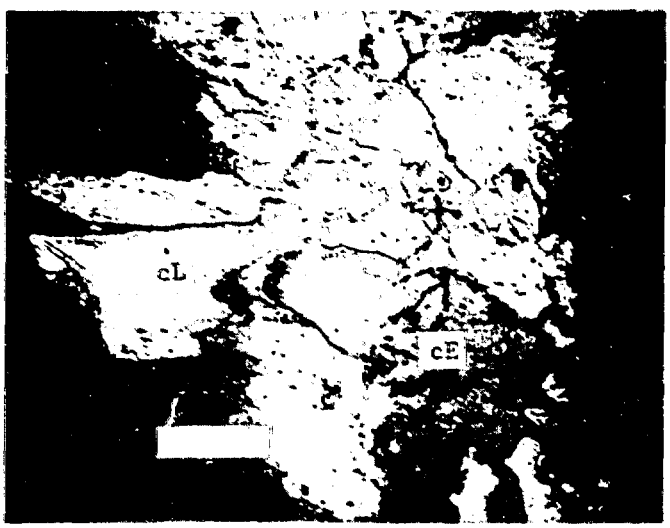

Coarse calcite crystals, subsampled to analyze both early compositions (cE) and later compositions (cL). Calcite forms on top of Ca-zeolite and vapor-phase crystals lining a fracture; details of intergrown and later-formed Ca-zeolite are shown in Fig. 8. Scale bar is 1 mm.

INAA analyses:

	early(cE)	late(cL)
CaO	55.4(9)%	55.6(1.1)%
Na	47(3)µg/g	47(5)µg/g
Sc	0.0064(3)	0.0162(3)
Cr	<2	<2
Fe	9(2)	19(2)
Co	<0.006	<0.010
Ni	<5	<6
Zn	6.0(1.5)	8(2)
As	1.48(9)	0.32(12)
Se	- -	- -
Br	0.10(4)	- -
Rb	0.6(2)	0.4(2)
Sr	94(5)	29(4)
Zr	<7	<7
Sb	0.006(2)	<0.01
Cs	0.262(6)	0.090(3)
Ba	7(2)	<25
La	17.2(2)	52.2(7)
Ce	0.16(4)	1.35(6)
Nd	26.7(1.1)	51(2)
Sm	7.52(11)	12.4(2)
Eu	0.390(6)	0.595(8)
Tb	1.52(2)	2.30(3)
Yb	2.42(3)	4.27(6)
Lu	0.336(5)	0.592(10)
Hf	0.031(7)	<0.03
Ta	0.004(2)	<0.01
W	<0.9	<0.7
Th	0.054(5)	0.481(11)
U	0.27(2)	0.13(4)
Au	<1.5 ng/g	<2 ng/g

APPENDIX: CALCITE PETROGRAPHY AND CHEMISTRY - 4

Sample USW G-2, 1640 m (LANL-262; HD-264)

electron microprobe analyses:

	dolomite cc1	calcite cc2	calcite cc4
CaO	30.4(2)	54.5(4)	54.6(4)
MgO	21.0(2)	0.42(2)	0.15(2)
FeO	0.00	0.06(4)	0.08(4)
MnO	0.25(3)	0.70(4)	1.19(5)
CO_2	48.4	44.3	44.0
Ca	0.498	0.973	0.979
Mg	0.481	0.010	0.004
Fe	0.000	0.001	0.001
Mn	0.003	0.010	0.017
C	1.012	1.008	1.006
Σ	1.994	2.002	2.007

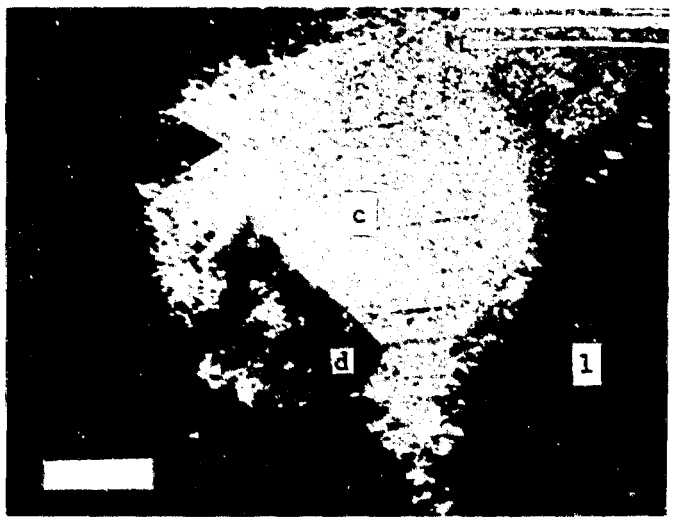

Calcite (c) with lesser amounts of intergrown dolomite (d) in a closed fracture; small crystals between the carbonates and the calcite- and albite-altered quartz-latite lava (l) are quartz. Scale bar is 1 mm.

INAA analysis:

CaO	54.8(9)%
Na	10(2)μg/g
Sc	5.94(8)
Cr	<1
Fe	148(7)
Co	0.644(14)
Ni	<25
Zn	12(2)
As	<0.3
Se	- -
Br	<0.3
Rb	<0.9
Sr	830(40)
Zr	<25
Sb	<0.03
Cs	<0.06
Ba	<20
La	4.79(7)
Ce	7.61(16)
Nd	4.8(1.1)
Sm	1.131(16)
Eu	0.680(12)
Tb	0.301(9)
Yb	1.27(2)
Lu	0.178(4)
Hf	<0.05
Ta	<0.02
W	<2
Th	<0.05
U	<0.2
Au	<3 ng/g

APPENDIX: CALCITE PETROGRAPHY AND CHEMISTRY - 5

Sample USW G-2, 1756 m (LANL-261; HD-265)

electron microprobe analyses:

	cc1	cc2	cc3
CaO	54.6(4)	55.1(4)	54.5(4)
MgO	0.10(2)	0.17(2)	0.00
FeO	0.40(5)	0.04(4)	0.16(4)
MnO	1.70(6)	0.51(4)	2.06(7)
CO_2	43.2	44.2	43.2
Ca	0.987	0.985	0.986
Mg	0.003	0.004	0.000
Fe	0.006	0.001	0.002
Mn	0.024	0.007	0.029
C	0.996	1.003	0.996
Σ	2.016	2.000	2.013

Calcite (c) with smaller (< 0.2 mm) crystals of intergrown quartz (q) in calcite- and albite-altered dacite lava. Scale bar is 1 mm.

*low CaO value of INAA separate is caused by ~5% quartz contamination.

INAA analysis:

CaO	50.3(8)%*
Na	36(3)µg/g
Sc	0.498(7)
Cr	<1
Fe	3880(54)
Co	0.135(3)
Ni	<5
Zn	1.3(3)
As	<0.2
Se	- -
Br	<0.15
Rb	<0.7
Sr	247(11)
Zr	<7
Sb	0.014(2)
Cs	0.046(4)
Ba	15(2)
La	6.45(9)
Ce	12.8(2)
Nd	6.6(5)
Sm	1.199(17)
Eu	0.097(2)
Tb	0.073(3)
Yb	0.083(5)
Lu	0.0111(9)
Hf	<0.02
Ta	<0.003
W	<0.6
Th	0.022(5)
U	<0.1
Au	<0.7 ng/g

APPENDIX: CALCITE PETROGRAPHY AND CHEMISTRY - 6

Sample USW GU-3, 295 m (LANL-228; HD-276)

electron microprobe analyses:

	cc1	cc2	cc3
CaO	56.4(4)	54.6(4)	55.5(4)
MgO	0.00	0.44(2)	0.00
FeO	0.04(4)	0.01(4)	0.01(1)
MnO	0.03(2)	0.00	0.01(2)
CO_2	43.5	45.0	44.5
Ca	1.013	0.966	0.986
Mg	0.000	0.011	0.000
Fe	0.001	0.000	0.000
Mn	0.000	0.000	0.000
C	0.995	1.015	1.007
Σ	2.009	1.992	1.993

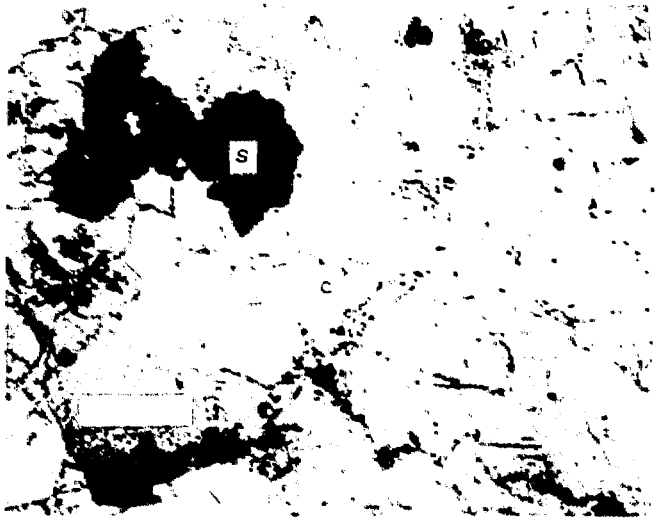

Coarse, subequant calcite crystals (c) with intergrown or texturally later-formed sepiolite and opal (s; details shown in Fig. 9). Euhedral fluorite also occurs in this sample, overgrown by calcite. Scale bar is 1 mm.

INAA analysis:

CaO	56.0(9)%
Na	12.6(3)µg/g
Sc	0.00190(7)
Cr	<1
Fe	4.7(1.0)
Co	0.0017(8)
Ni	<2
Zn	1.2(2)
As	0.542(16)
Se	- -
Br	0.033(9)
Rb	<0.19
Sr	241(11)
Zr	<3
Sb	<0.004
Cs	0.018(2)
Ba	<7
La	0.751(11)
Ce	<0.15
Nd	2.6(3)
Sm	0.884(13)
Eu	0.0122(8)
Tb	0.286(5)
Yb	0.748(11)
Lu	0.0928(16)
Hf	<0.02
Ta	<0.003
W	<0.4
Th	0.017(5)
U	0.175(8)
Au	<1 ng/g

APPENDIX: CALCITE PETROGRAPHY AND CHEMISTRY - 7

Sample USW GU-3, 313 m (LANL-266; HD-267)

electron microprobe analysis:

	cc1
CaO	56.2(4)
MgO	0.43(2)
FeO	0.00
MnO	0.03(3)
CO_2	43.3
Ca	1.008
Mg	0.011
Fe	0.000
Mn	0.000
C	0.990
Σ	2.009

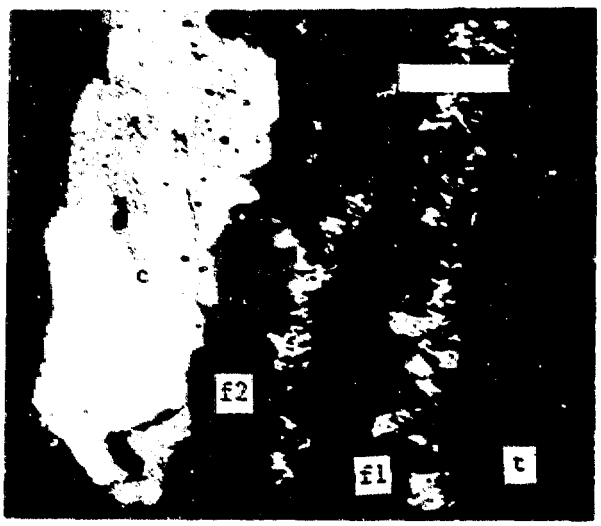

Coarse calcite (c) formed over clear fluorite (f2); cloudy fluorite (f1) also occurs in this sample. Vapor-phase crystals line the fracture surface between the fluorite and the tuff (t). Scale bar is 1 mm.

INAA analysis:

CaO	56.4(9)%
Na	9.9(4)µg/g
Sc	0.00181(12)
Cr	<0.3
Fe	3.4(9)
Co	<0.004
Ni	<2
Zn	0.9(2)
As	0.29(2)
Se	- -
Br	0.017(7)
Rb	<0.3
Sr	338(12)
Zr	<3
Sb	<0.005
Cs	0.0074(15)
Ba	<7
La	0.641(9)
Ce	<0.1
Nd	1.7(3)
Sm	0.559(8)
Eu	0.0140(7)
Tb	0.190(3)
Yb	0.517(8)
Lu	0.0640(14)
Hf	<0.02
Ta	<0.003
W	<0.3
Th	0.013(5)
U	0.126(10)
Au	0.4(2)ng/g

APPENDIX: CALCITE PETROGRAPHY AND CHEMISTRY - 8

Sample USW GU-3, 347 m (LANL-236; HD-278)

electron microprobe analyses:

	cc1	cc2
CaO	55.4(4)	55.5(4)
MgO	0.00	0.00
FeO	0.03(4)	0.00
MnO	0.00	0.00
CO_2	44.6	44.5
Ca	0.984	0.987
Mg	0.000	0.000
Fe	0.000	0.000
Mn	0.000	0.000
C	1.010	1.009
Σ	1.994	1.996

Coarse calcite (c); a thin layer of fluorite (f) occurs between the calcite and the vapor-phase crystals that line this fracture in devitrified tuff. Scale bar is 1 mm.

INAA analysis:

CaO	55.1(9)%
Na	28.2(1.0)µg/g
Sc	0.0268(4)
Cr	<1
Fe	9.2(1.2)
Co	0.0101(13)
Ni	<2
Zn	1.4(3)
As	0.42(4)
Se	- -
Br	0.06(3)
Rb	<0.4
Sr	120(7)
Zr	<3
Sb	<0.02
Cs	0.036(3)
Ba	<8
La	0.938(13)
Ce	0.15(4)
Nd	3.0(4)
Sm	0.819(12)
Eu	0.0341(13)
Tb	0.310(5)
Yb	1.32(2)
Lu	0.179(3)
Hf	<0.02
Ta	<0.004
W	<0.2
Th	0.023(6)
U	0.061(16)
Au	<0.7 ng/g

APPENDIX: CALCITE PETROGRAPHY AND CHEMISTRY - 9

Sample USW GU-3, 358 m (LANL-238; HD-279)

electron microprobe analyses:

	cc1
CaO	56.1(4)
MgO	0.00
FeO	0.00
MnO	0.01(2)
CO_2	43.9
Ca	1.003
Mg	0.000
Fe	0.000
Mn	0.000
C	1.001
Σ	2.004

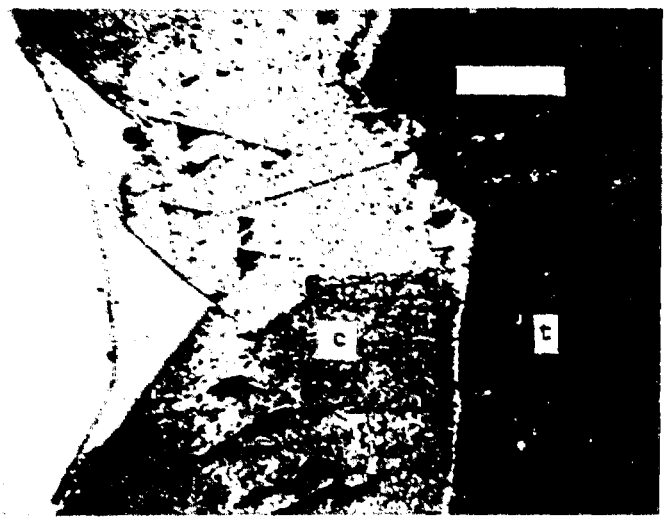

Coarse calcite (c) formed over vapor-phase crystals that line a fracture in devitrified tuff (t). Scale bar is 1 mm.

INAA analysis:

CaO	55.4(9)%
Na	10.7(4)μg/g
Sc	0.00507(16)
Cr	0.28(11)
Fe	9(2)
Co	0.020(2)
Ni	<3
Zn	1.2(2)
As	0.09(4)
Se	0.15(7)
Br	0.045(17)
Rb	<0.4
Sr	151(10)
Zr	<5
Sb	<0.006
Cs	0.040(3)
Ba	<8
La	0.469(7)
Ce	<0.2
Nd	2.3(8)
Sm	0.492(7)
Eu	0.0109(9)
Tb	0.175(4)
Yb	0.850(13)
Lu	0.122(2)
Hf	<0.02
Ta	<0.003
W	0.10(4)
Th	0.018(7)
U	<0.1
Au	1.0(2)ng/g

APPENDIX: CALCITE PETROGRAPHY AND CHEMISTRY - 10

Sample USW G-3, 1464 m (LANL-269; HD-270)

electron microprobe analyses:

	cc1	cc2
CaO	51.1(4)	49.1(4)
MgO	0.00	0.12(2)
FeO	0.14(4)	0.65(6)
MnO	4.73(10)	5.77(11)
CO_2	44.0	44.4
Ca	0.918	0.881
Mg	0.000	0.003
Fe	0.002	0.009
Mn	0.067	0.082
C	1.007	1.015
Σ	1.994	1.990

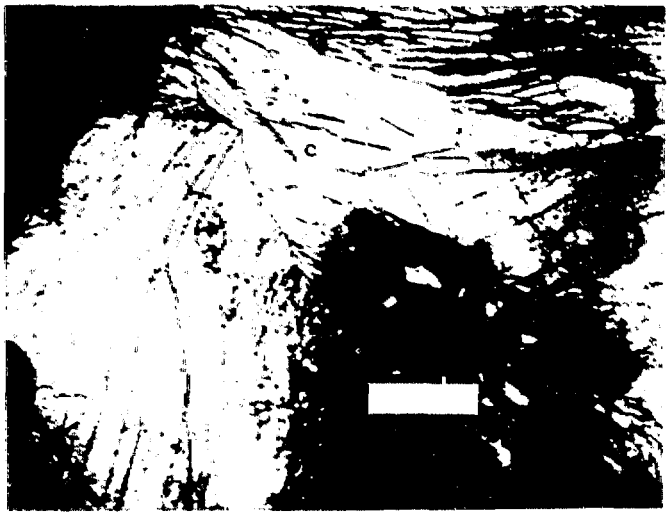

Coarse calcite crystals (c) from a closed fracture in analcime-altered tuff. Scale bar is 1 mm.

INAA analysis:

CaO	50.2(8)%
Na	19(5)µg/g
Sc	1.55(2)
Cr	<2
Fe	3190(50)
Co	0.021(4)
Ni	<11
Zn	10(2)
As	0.21(9)
Se	- -
Br	<0.16
Rb	<0.9
Sr	111(10)
Zr	<15
Sb	0.010(5)
Cs	0.021(7)
Ba	<9
La	31.0(4)
Ce	57.9(8)
Nd	26.7(1.2)
Sm	7.21(10)
Eu	0.906(15)
Tb	2.27(3)
Yb	5.18(7)
Lu	0.625(9)
Hf	<0.03
Ta	<0.010
W	<0.6
Th	1.020(16)
U	<0.1
Au	<1.6 ng/g

Data Sources:

Notebook TWS-EES-1-12-90-4, pp. 1-12, 39-50, 86-103.

Notebook TWS-EES-1-5-92-3, pp. 1-13, and associated SEM images and electron microprobe output.

Notebook TWS-EES-1-2-93-6, pp. 27-28, 49-50.